water

MDPI

Article

Flow Characteristics in the Wake Region of a Finite-Length Vegetation Patch in a Partly Vegetated Channel

Didem Yılmazer [1], Ayşe Yüksel Ozan [2,*] and Kubilay Cihan [3]

[1] Civil Engineering Department, Namık Kemal University, Çorlu 59860, Tekirdag, Turkey; didem_yilmazer@yahoo.com
[2] Civil Engineering Department, Adnan Menderes University, Aydın 09010, Turkey
[3] Civil Engineering Department, Kırıkkale University, Kırıkkale 71450, Turkey; kubilaycihan@gmail.com
* Correspondence: ayse.yuksel@adu.edu.tr; Tel.: +90-256-213-7503 (ext. 3550)

Received: 26 February 2018; Accepted: 8 April 2018; Published: 11 April 2018

Abstract: Aquatic vegetation in rivers and coastal regions controls the flow structure in terms of mean velocity and turbulence. The vegetation in the flow affects the transportation of nutrients, microbes, dissolved oxygen, sediment, and contaminants; therefore, the flow characteristics of different types of vegetation layers should be examined in order to understand the effects of vegetation on the flow structure. In this paper, the effect of the submergence ratio and SVF (Solid Volume of Fraction) of a vegetation patch, which was present across half of the channel in a spanwise direction, on the flow structure at the wake region was examined. For this purpose, different submergence ratios with different SVFs were considered in the experiments, and velocity measurements were performed in the wake region of the vegetation layer with an Acoustic Doppler Velocimeter (ADV). According to the results, the effect of different vegetation heights and SVFs on the velocity distribution was obtained. Moreover, inflectional velocity distribution over the cross-section in the wake region of the vegetation layer was obtained, and it was concluded that jet flow occurred in the non-vegetated half of the channel due to the vegetation layer.

Keywords: vegetation patch; wake region; submerged ratio; SVF

1. Introduction

Vegetation has an important role in the sustainable development of the aquatic environment since it significantly affects the hydrodynamic characteristics of the flow. By altering the hydrodynamic conditions, submerged aquatic vegetation can dramatically affect the fate and transport of sediment, nutrients, contaminants, dissolved oxygen, and fauna in aquatic systems [1,2]. Vegetation in the aquatic environment is also very important for river management and the river environment. Thus, the investigation of the velocity distribution, turbulence structure as well as mass and momentum exchange between the vegetated and non-vegetated zones is a crucial issue for the river habitat.

In flows through submerged vegetation, the vertical discontinuity of the drag results in strong velocity shear at the top of the canopy and greatly increases the turbulence intensities in this region, relative to unobstructed flow [3–5]. Furthermore, coherent canopy-scale eddies have been observed to dominate vertical momentum fluxes into terrestrial [6–8], and aquatic canopies [5,9].

Vegetation reduces the suspended sediment transport as a result of the local reduction in bed shear stress [10]. Submerged vegetation generates coherent motions at the vegetation edge and such large-scale eddies control the vertical exchange of mass and momentum both within and above the vegetation layer [10].

Okamoto and Nezu (2013) [10] emphasized that a key feature of vegetation flow is the generation of a shear layer at the vegetation edge which is similar to the free shear layer. For aquatic vegetation flow, the flow structure has a range of behaviors depending on the submergence depth ratio [10].

Ghisalberti and Nepf (2004) [11] studied the dynamic equilibrium that occurred in a submerged vegetated shear layer and demonstrated that the turbulence kinetic energy in the shear layer was balanced by drag dissipation. They also presented a one-dimensional approximation of a three-dimensional flow for shear layer hydrodynamics.

Ghisalberti and Nepf (2006) [12] performed an experimental study on the structure of coherent vortices and vertical transport in shallow vegetated shear flows using rigid and flexible vegetation models. They implied that environmental flows over porous media, boulder beds, urban landscapes, wind farms, agricultural, and forest canopies were examples of an obstructed shear flow like flow over submerged vegetation. They also figured out that the vortex street in a vegetated shear layer created a pronounced oscillation in the velocity profiles. Moreover, the oscillation in vegetation had the effect of decreasing the amount of the turbulent vertical momentum transportation in the shear layer when compared to the flow over rigid vegetation [12].

Nepf (1999) [2] developed a model that predicted the turbulence intensity and diffusion within emergent vegetation. This model showed that turbulence intensity was dependent on the vegetative drag and for lower densities, which were smaller than 0.01, the bed-drag and bed-shear production were negligible when compared to their vegetation correspondents. They also found that the turbulence scales were controlled by vegetation geometry, especially for vegetation densities higher than 0.01 [2].

Ben Meftah et al. (2014) [13] presented a new theoretical approach to model the flow pattern within the shear layer in the unobstructed area close to the vegetated area. They validated their model with experiments using rigid emergent vegetative elements for different Reynolds numbers. They showed that the peak of the turbulence intensity and that of the spanwise Reynolds Stress were shifted toward the center of the shear layer.

Ben Meftah and Mossa (2016) [14] focused on the effect of the contraction ratio, which is the ratio between the width of the obstructed and unobstructed area in the flow hydrodynamic structure. They found that the contraction ratio affected the flow hydrodynamic, and also presented an improved modified log-law that predicted the transversal profile of the mean flow velocity at the interface of obstructed and unobstructed areas.

Nepf and Vivoni (2000) [15] performed a study on the transition between submerged and emergent canopy flows. They suggested that the flow within an aquatic canopy could be divided into two regions: upper and lower. In the upper canopy, which is the "vertical exchange zone", vertical turbulence exchange with the overlying water is dynamically significant to the momentum balance and turbulence; and turbulence produced by mean shear at the top of the canopy is important [15]. The lower canopy, the "longitudinal exchange zone", communicates with surrounding water predominantly through longitudinal advection [15]. Nepf and Vivoni (2000) [15] indicated that in the lower layer, turbulence was locally generated by the canopy elements, and the momentum budget was a simple balance of vegetative drag and pressure gradient. They also emphasized that a vertical exchange zone appeared at the top of the canopy and deepened into the canopy as the depth of submergence increased in the submerged canopy.

Poggi et al. (2004) [16] developed a phenomenological model that described the turbulence structure within the canopy shear layer by using Laser Doppler Anemometry (LDA) measurements. They divided the canopy sublayer into three zones: the deep zone, where the Karman vortices drive the flow; the second zone, which is the mixing layer; and the uppermost zone where the classical surface-layer similarity theory was present (Figure 1).

Aquatic vegetation occurs in patches of finite length and different submergence ratios in natural rivers. In such vegetated flows, flow is diverted away from the vegetation patch at the leading edge of the patch [10]. In these areas, a shear layer does not form, and longitudinal advection contributes significantly to mass and momentum transport [10].

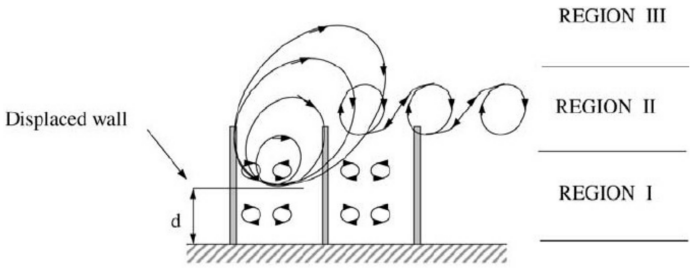

Figure 1. Regions of the canopy sub-layer [16].

Aside from experimental and analytical studies, there have also been numerical studies about vegetation in open channel flows. Brito et al. (2016) [17] studied open channel flows with submerged vegetation floodplains numerically. They modeled the vegetation layer as a porous media and demonstrated that the anisotropic turbulence EARSM (Explicit Algebraic Reynolds Stress Model) model was able to reproduce the secondary currents.

Kang and Choi (2006) [18] described a Reynolds stress model for the numerical simulation of compound open-channel flows with submerged vegetation on the floodplain. They considered various sub-models in the numerical model. Moreover, they also investigated lateral momentum transfer in the compound-open channel and demonstrated that the rate of change of the apparent shear stress increased with vegetation density. Additionally, with the increasing vegetation density on the floodplain, the drag force term was pronounced when compared with the lateral gradient of the apparent shear stress and to reduce the bottom shear stress of its 2D value in the floodplain [18].

The motivation behind this study was to examine the effect of the submergence ratio of the vegetation patch with different vegetation SVFs on the flow structure at the wake region of the patch. For this purpose, different submergence ratios with different SVFs were considered. This study especially focused on the wake region of the vegetation layer at the partly vegetated channel. The velocity measurements in the flow area were conducted with Acoustic Doppler Velocimeter (ADV).

2. Experimental Method

Experiments were conducted in an 11 m long, 1.2 m wide, and 0.75 cm deep flume with glass walls in the Civil Engineering Laboratory at Adnan Menderes University (Figures 2 and 3). The flume had an interior re-circulating system providing a steady flow. Figure 2a shows the schematic of the experimental set-up. Flow depths were measured by means of a pointer gauge and the velocity measurements were performed by SONTEK Acoustic Doppler Velocimeter (ADV). Bricks were installed along the cross section of the flume at the entrance and outlet of the flume to provide smooth inlet and outlet conditions.

The entire base of the flume was covered with a plywood sheet and a finite-length submerged vegetation patch was composed with d = 0.01 m diameter rigid circular plastic rods in a plywood sheet. The rods had two different heights: h_{v1} = 0.05 m, and h_{v2} = 0.10 m. The cylinders in the vegetation patch were placed in a staggered, equilateral array. For this geometry, the solid volume fraction was related to the spacing (s) and diameter (d) by White and Nepf, 2007 [19]:

$$\varnothing = \left(\sqrt{3}\pi/6\right)\left(d^2/s^2\right) \quad (1)$$

In these experiments, the vegetation layer was characterized by the solid volume fraction-SVF (ϕ_1) and the height of the vegetation layer (h_v). The variable ϕ was defined as the ratio of volume occupied by the cylinders to the total volume of vegetation layer. Experiments were performed for two different SVFs, ϕ_1 = 0.01 and ϕ_2 = 0.08, and two different vegetation heights, h_{v1} = 0.05 m and h_{v2} = 0.10 m. Here, ϕ_1 = 0.01 and ϕ_1 = 0.08 corresponded to N_1 = 172 IP/m^2, and N_2 = 1142 IP/m^2 respectively, where IP/m^2 means the individual plant number per square meter. Moreover, the blockage caused by

the vegetation layer was characterized by its frontal area per volume (V_0), called the vegetation layer density, a (m^{-1}) [20]. Vegetation density was calculated with the given equation;

$$a = A/V_0 = nh_v d/h_v S \quad (2)$$

where A is the frontal area of a vegetation element; h_v is the vegetation height; n is the number of the vegetation elements occupied in the referred bed area S; and H is water depth.

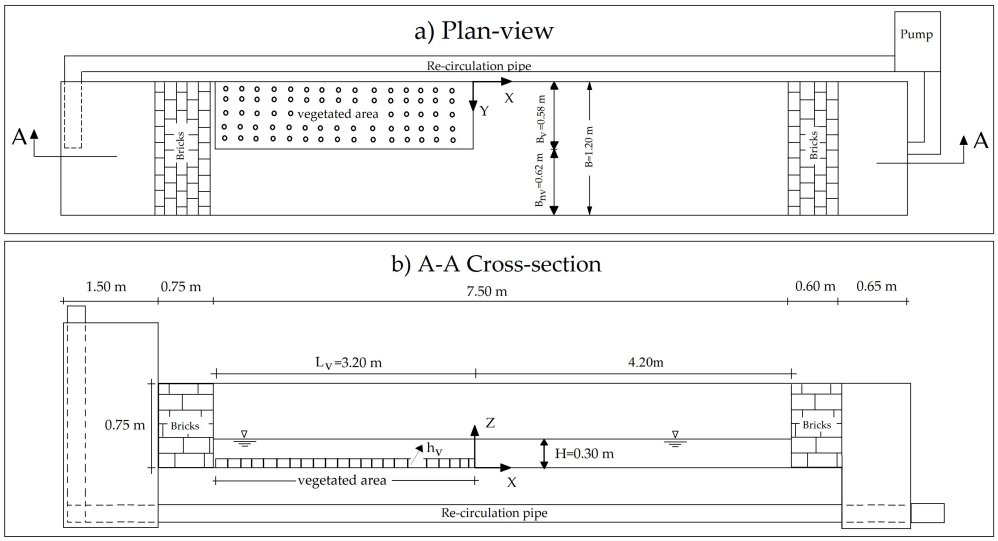

Figure 2. Schematic views of the channel: (**a**) Plan view of the flume; (**b**) A-A cross-section of the flume.

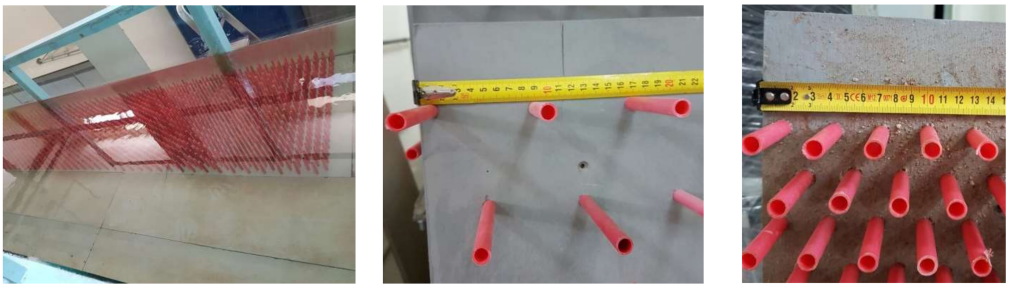

(**a**) (**b**) (**c**)

Figure 3. Photos from experimental set-up: (**a**) Vegetation layer in the flume; (**b**) vegetation layer with ϕ_1 = 0.01; (**c**) vegetation layer with ϕ_2 = 0.08.

For all cases, the water depth, H = 0.30 m, and bulk mean velocity were kept constant. The Reynolds Number $\left(\mathrm{Re} = u_{dm}H/\nu = 41,000\right)$ and Froude Number $\left(\mathrm{Fr} = u_{dm}/\sqrt{gH} = 0.08\right)$ were calculated using the mean depth averaged velocity (u_{dm}) for the non-vegetated case. Here, H is flow depth; ν is the kinematic viscosity; and g is the gravitational acceleration. Mean depth averaged velocity (u_{dm}) for the non-vegetated case was used for the non-dimensionalization of the figures in Section 3. Table 1 shows the hydraulic conditions.

Table 1. Hydraulic conditions.

Cases	N (IP/m^2)	ϕ	λ (ah)	h_v (cm)	H/h_v	u_{dm} (cm/s)
h5f1	172	0.01	0.08	5	6	13.6
h5f8	1142	0.08	0.57	5	6	13.6
h10f1	172	0.01	0.17	10	3	13.6
h10f8	1142	0.08	1.14	10	3	13.6

The three instantaneous components of velocity (u, v, w), corresponding to the streamwise, spanwise and vertical velocity components in X, Y and Z directions, respectively, were measured with ADV during 120 s with 3000 sampling number at 25 Hz. Each velocity record was decomposed into time averages ($\overline{u}$, $\overline{v}$, $\overline{w}$) and fluctuating components (u', v', w'). The ADV probe was established over the vegetation layer during the experiments. The velocity measurements were performed at 117 (=9 × 13) points in the XY plane (Figure 4a) and six different levels in the Z direction (Figure 4b). Measurement points along the X and Y directions were placed at 10 cm intervals and 2.5 cm in the Z direction. Only, point Z1 (=0.05 cm) was placed at the closest point to the wall where the velocity measurement could be performed (Figure 4b).

ADV measurements sometimes may include scattering data because of using clean water without suspended material and correlation scores. If the correlation factor of measured velocities are very low then velocity measurements can not be reliable. The manufacturer recommends that a 15 db signal-to-noise ratio (SNR) and a correlation coefficients larger than 70% for high-resolution measurements. Therefore, the poor quality samples in the measured data were removed using SNR < 15 db and correlation coefficient < 70% conditions.

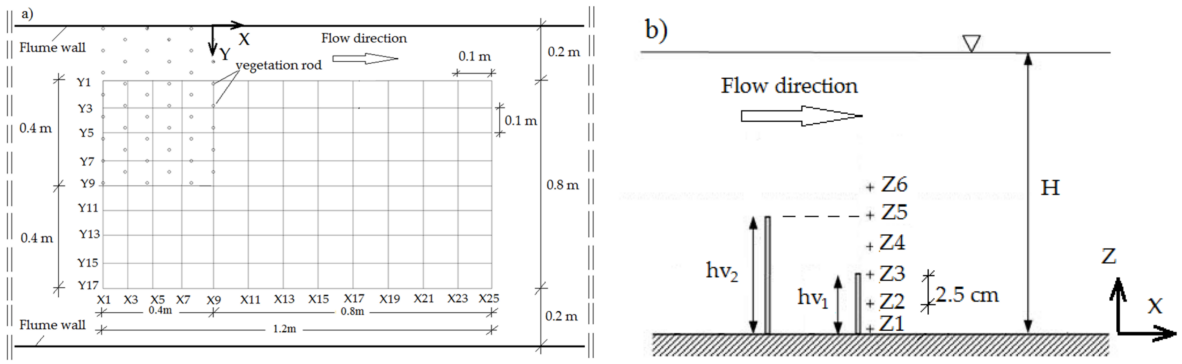

Figure 4. Velocity measurements grid: (**a**) Plan-view; (**b**) Side-view.

3. Results and Discussion

Figure 5 presents the non-dimensional velocity distributions for the non-vegetated case along the vertical direction at different sections of the channel and logarithmic velocity distribution. It could be seen that the streamwise velocity distribution represented the best fitted logarithmic regression line for the non-vegetated case. The logarithmic line was obtained by using the law [21] for rough boundaries, which is

$$\frac{u}{u_*} = \frac{1}{\kappa} ln\left(\frac{30z}{k_s}\right) \quad (3)$$

where u is streamwise point velocity; u_* is local shear velocity; κ is von Karman's constant; z is distance from the measurement point to the bed; and k_s is the Nikuradse equivalent bed roughness. Velocity profiles, which were plotted on semi-logarithmic paper, fitted the logarithmic law display as a constant gradient [22,23].

Figure 6 presents an example of a measured velocity for non-vegetated case (Figure 6a) and spectral distribution (Figure 6b) for h_{v2} = 0.10 m at X13Y3Z2. This point corresponds to the wake region of the vegetated layer. Velocity range was chosen as ±0.3 m/s with a velocity accuracy of ±1 in the measurements. A signal-to-noise ratio (SNR) higher than 15 dB is recommended for 25 Hz and higher sample rates, and the typical threshold for data acceptance is a correlation coefficient higher than 70% for high-resolution measurements [24]. Therefore, the measured data were filtered with Phase-space threshold despiking [25,26] which is the default filter in winADV and poor quality samples were removed using SNR < 15 dB and correlation coefficient < 70%.

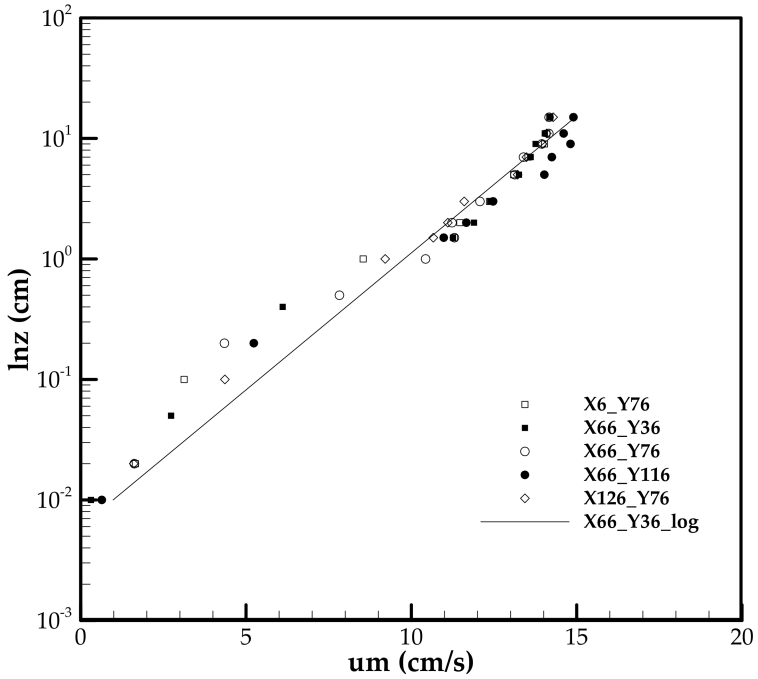

Figure 5. Velocity profiles in semi-logarithmic form for non-vegetated case at different sections of the channel.

In order to explore the distribution of energy in the signal across frequencies, examples of the power spectral densities (PSD) of velocity fluctuations in three directions were plotted in Figure 6b. The spectrum frequency between 0.2 and 0.6 Hz which indicates the scaling subrange is referred to as the production subrange. This range is characterized by a $-3/2$ spectral slope [27]. An inertial subrange with a $-5/3$ power law between 0.9 and 5 Hz which is in a narrow range was observed. There is transitional subrange between 0.6 and 0.9 Hz which corresponds to transition between the production subrange and the inertial subrange. In the transition subrange, a transformation of the turbulent energy of large scale motion to energy of small scale motion takes place [27]. The PSD has small values at a frequency highger than 5 Hz, which corresponds to the universal equilibrium range. These results are in agreement with results obtained by Meftah and Mossa [27] and Nezu and Onitsuka [28].

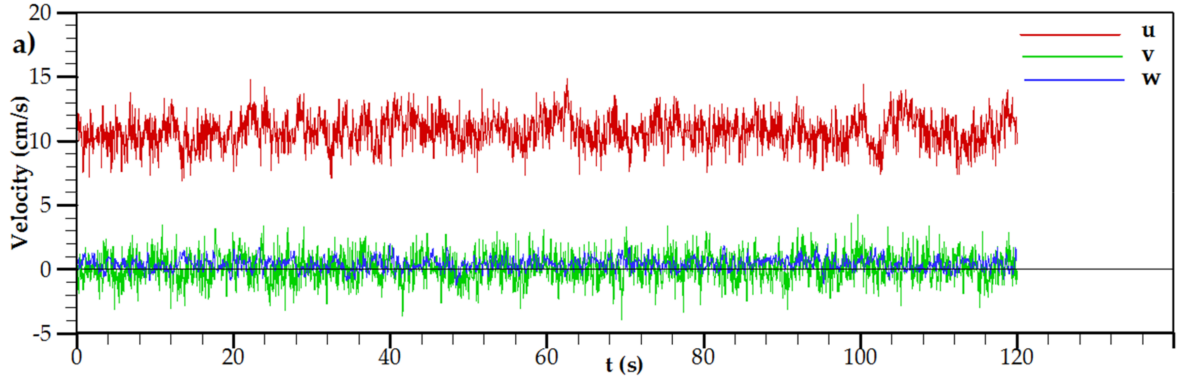

Figure 6. *Cont.*

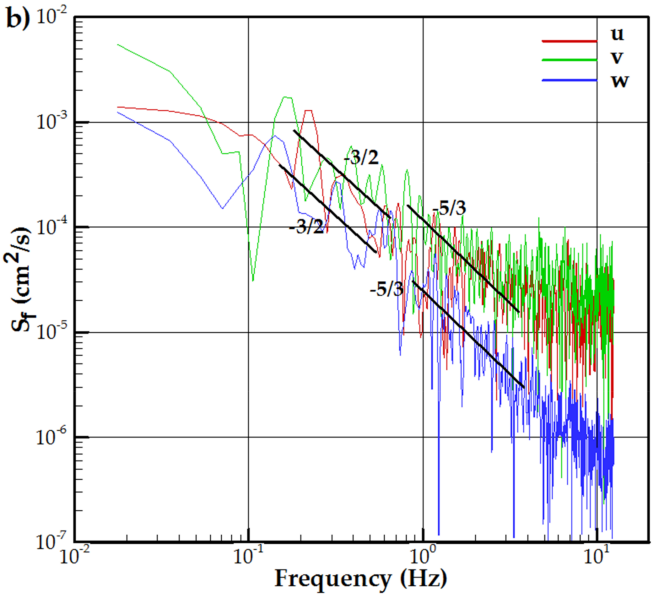

Figure 6. (**a**) Measured velocity signal at X13Y3Z2 for non-vegetated case; (**b**) Spectral distribution at X13Y3Z2 for h_{v2} = 0.10 m.

Figure 7 shows the non-dimensional streamwise velocity distributions along the vertical direction at different spanwise (Y3, Y9, and Y15) and streamwise (X1, X5, X9, X13, X17, and X25) sections for h_{v1} = 0.05 m and h_{v2} = 0.10 m with ϕ = 0.08, respectively. Here, Y3, X1, and X5 corresponded to the vegetated area whereas Y9 and X9 corresponded to the edge of the vegetation layer (Figure 4a). Additionally, Y15 was placed in the non-vegetated half of the channel whereas X13, X17, and X25 were placed at the wake region of the vegetated layer (Figure 4a). It was obvious that the vegetation layer decreased velocity both inside the vegetation layer and also in the wake region (Figure 7a). Furthermore, the velocity decreased inside and in the wake region of the vegetation layer while it had the same value as the non-vegetated case downstream of the vegetated area (Figure 7b). Moreover, the velocity increased to remain off the vegetation layer (Figure 7c). This increase occurred at about 20% for h_{v2} and 10% for h_{v1}. Furthermore, the velocity difference increased between the vegetated and non-vegetated cases, which was higher for higher vegetation height even when both cases had the same SVF. The main conclusion from these figures was that the velocity decrease occurred in the wake of the vegetation patch whereas velocity increase, which refers to jet flow, occurred along the unobstructed part of the channel.

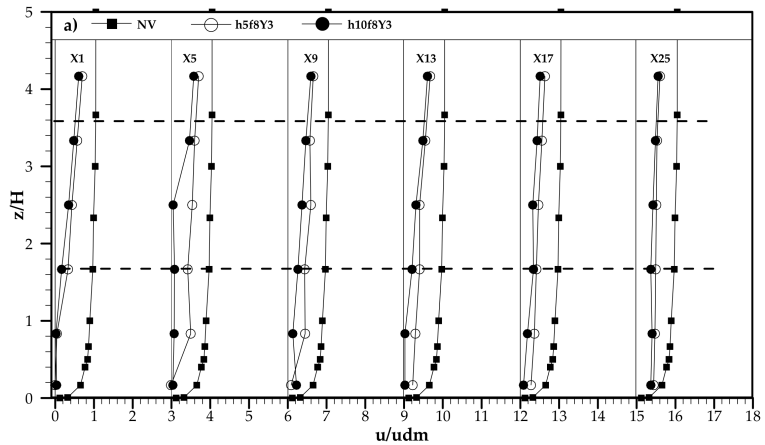

Figure 7. *Cont.*

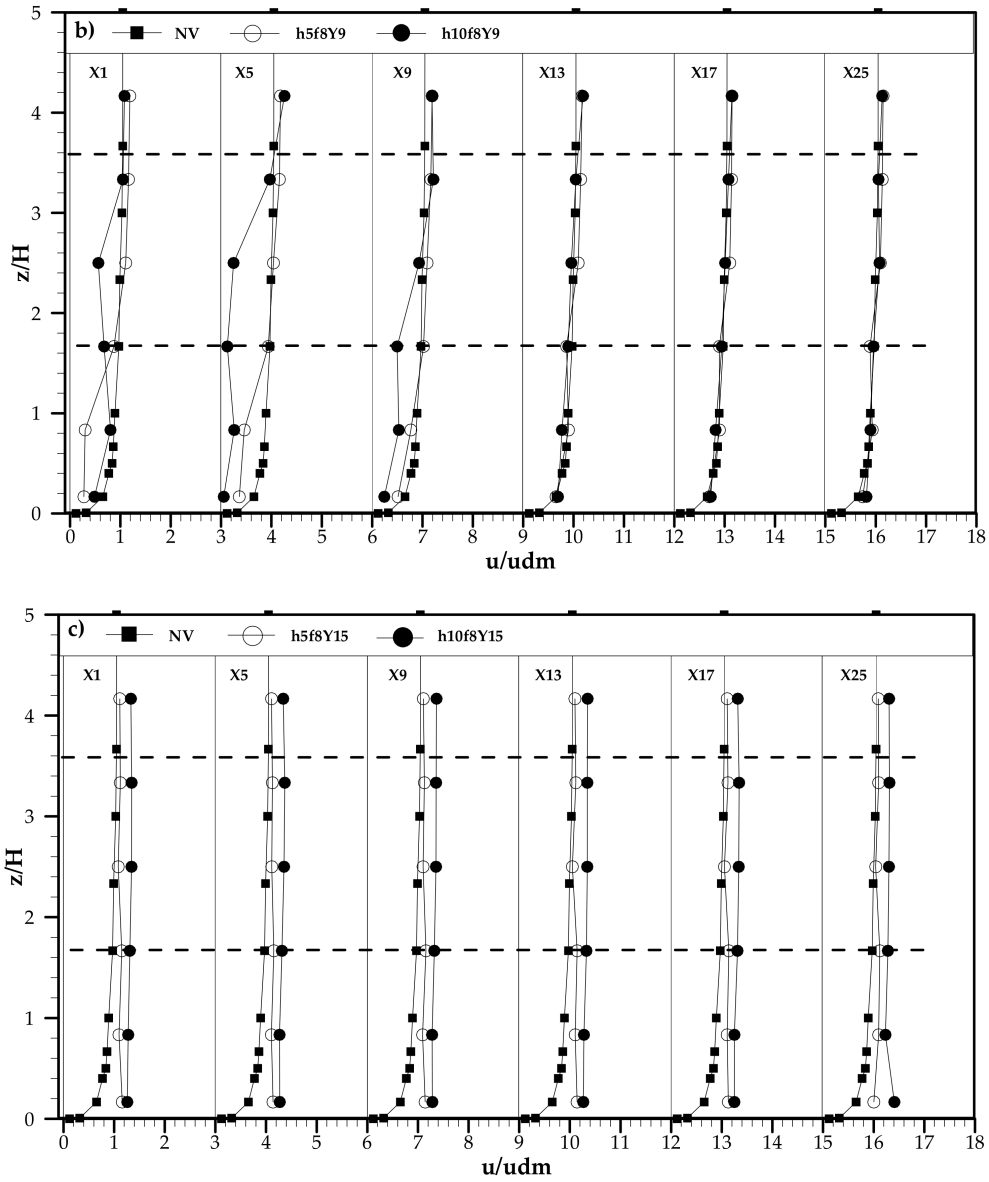

Figure 7. Non-dimensional streamwise velocity distributions along vertical direction at different streamwise sections for both vegetation heights and ϕ = 0.08: (**a**) Y3; (**b**) Y9; (**c**) Y15.

Yang et al. (2007) [29] studied the flow patterns in a compound channel with vegetated floodplains and used different types of artificial submerged vegetative elements in the experiments distribution on the floodplain. They also found similar velocity distributions for the vegetated flood plain where velocity decreased, and the non-vegetated main channel where velocity increased for compound open-channels.

Figure 8 presents the non-dimensional streamwise velocity distributions at the Y3 line along the streamwise direction for h_{v1} = 0.05 m and h_{v2} = 0.10 m with different SVFs. Here, Z2 and Z6 corresponded to the point at the half of the vegetative height, and Z4 and Z6 corresponded to the point over the vegetation layer. It could be seen that low SVF had little effect on the velocity distribution over the vegetation while higher SVF had a large effect, which was an important decrease in velocity distribution inside the vegetation layer for h_{v1} = 0.05 m. However, with the higher vegetation height (h_{v2} = 0.10 m), the vegetation layer affected the velocity distribution both within and over the vegetation layer. Within the vegetation layer, both SVF values caused a velocity decrease whereas the effect was larger for higher SVF. However, velocity values overlapped to remain off the vegetation layer, especially

in the wake region for h_v = 0.05 m vegetation height. However, this was not observed for higher vegetation height (h_{v2} = 0.10 m). Velocity decrease occurred in about 50% of the wake region for higher SVF for both vegetation height cases.

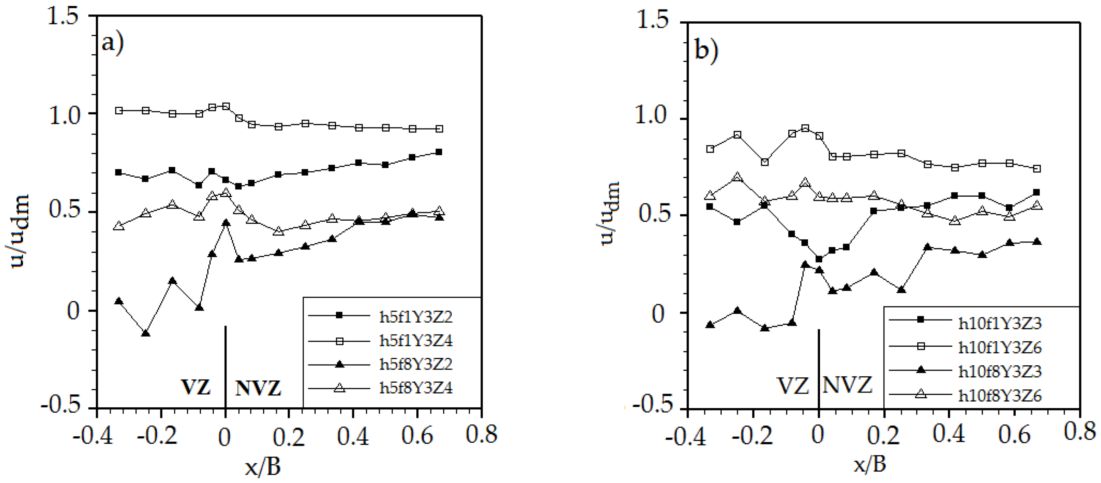

Figure 8. Non-dimensional streamwise velocity distributions at Y3 line along the streamwise direction for different SVFs, (**a**) h_{v1} = 0.05 m; (**b**) h_{v2} = 0.10 m.

Figures 9 and 10 show the non-dimensional streamwise velocity distributions along the spanwise direction at different sections of the wake region for z/h_v = 0.5 and z/h_v = 1.5, respectively. The figures are for lower vegetation height (h_{v1} = 0.05 m) and different SVFs. It was found that higher SVF decreased the flow velocity more than the lower SVF for outer layer of the vegetation zone (Figure 10). Apart from this, velocity decrease was similar for both SVFs close to the bed (Figure 9). It was also observed that close to the bed (z/h_v = 0.5), the velocity decrease continued further out of the vegetated area (y/B ≅ 0.7). However, the velocity decrease disappeared at the vegetation edge and velocity started to increase over the vegetation layer along the spanwise direction. The effect of SVF over the vegetation layer can be seen remarkably in Figures 9 and 10. The velocity decrease was still present over the vegetation layer, and the effect of vegetation was still present in the other half of the channel. Moreover, the velocity difference was about 0.5–0.6 u_m for both Z2 and Z4 between the vegetated and non-vegetated zones of the flow over the cross-section. However, the main difference was that the velocity was higher than the non-vegetated case at about 1.2 u_m for Z2 where it was about 1.1 u_m for Z4 at the non-vegetated zone. This gives an idea about the occurrence of jet flow at the non-vegetated zone of the flow. Additionally, a higher SVF caused a higher drag force, which can be clearly seen in Figure 10 where the higher SVF had smaller velocity values at both zones of the flow. Another important feature obtained from Figure 10 was the inflectional velocity profile over the cross-sections, and the velocity profile had a steep shape for higher SVF over the vegetation layer. This type of velocity distribution also implied that jet flow occurred in the non-vegetated half of the channel. This jet flow was present in all parts of the non-vegetated zone, even starting inside the vegetation layer, which was close to the vegetation edge at z/h_v = 1.5 where it started at (y/B ≅ 0.7) close to the bed (z/h_v = 0.5). Nezu and Onitsuka (2001) [28] performed measurements on partly vegetated open-channel flows and also found similar results over the cross-section. The difference of this study is that the results were given for the wake region. Ikeda et al. [30,31] demonstrated that this type velocity profile showed a generation of coherent horizontal vortex due to an inflectional instability.

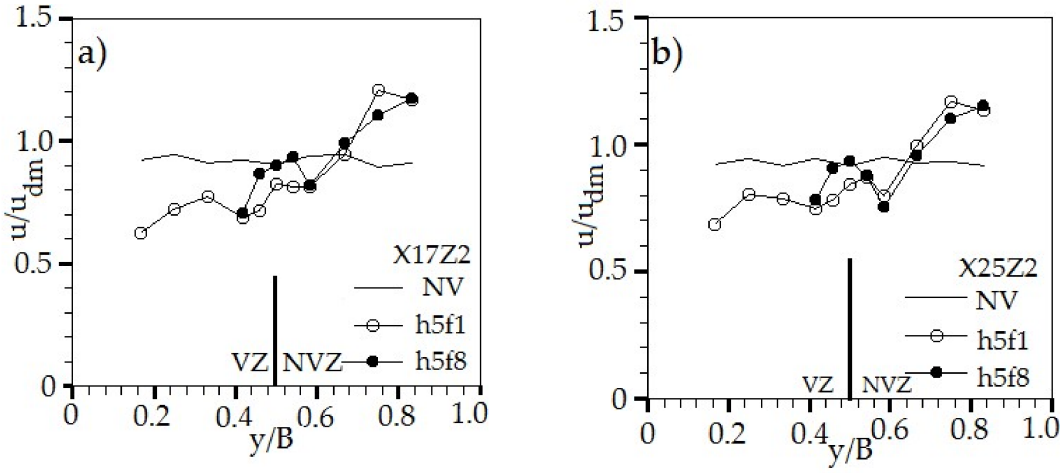

Figure 9. Non-dimensional streamwise velocity distributions along the spanwise direction at z/h_v = 0.5 for h_v = 0.05 m and different SVFs; (**a**) X17; (**b**) X25.

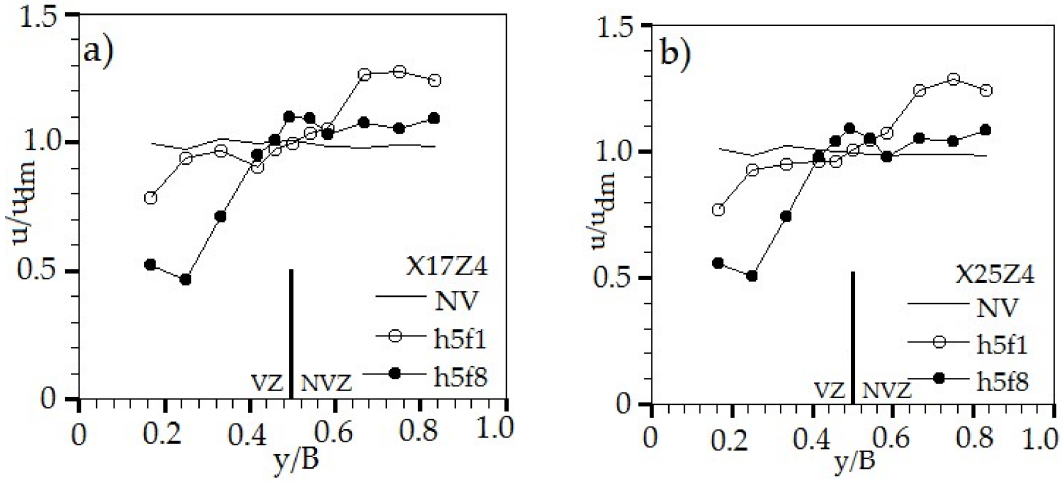

Figure 10. Non-dimensional streamwise velocity distributions along the spanwise direction at z/h_v = 1.5 for h_v = 0.05 m and different SVFs; (**a**) X17; (**b**) X25.

Figures 11 and 12 show the non-dimensional streamwise velocity distributions along the spanwise direction at different streamwise sections for z/h_v = 0.5 and z/h_v = 1.25, respectively. The figures are for higher vegetation height (h_v = 0.10 m) and different SVFs. Figure 11 presents the velocity distribution close to the bed, which was within the vegetation layer, and the velocity distribution here showed similar behavior to the velocity distribution over the vegetation layer for lower vegetation height. Still, there was a steeper inflectional velocity distribution for higher SVF. However, here there was an important difference from lower vegetation height. The difference was that in the non-vegetated zone of the channel, the velocity values were higher for higher SVF than the lower SVF. Moreover, the velocity difference was about 0.7–0.8 u_m for lower SVF where it was 1.0–1.1 u_m for higher SVF at both Z3 and a Z6 between the vegetated and non-vegetated zones of the flow over the cross-section. Another important result was that the velocity increase ratio was almost the same for both SVF at the non-vegetated zone where the velocity decrease ratio was higher for higher SVF in the vegetated zone, which was about 0.2 u_m. The other difference was that the velocity increase started at the junction between the vegetated and non-vegetated zones for higher SVF and at the non-vegetated zone, which was about y/B~0.7 for lower SVF.

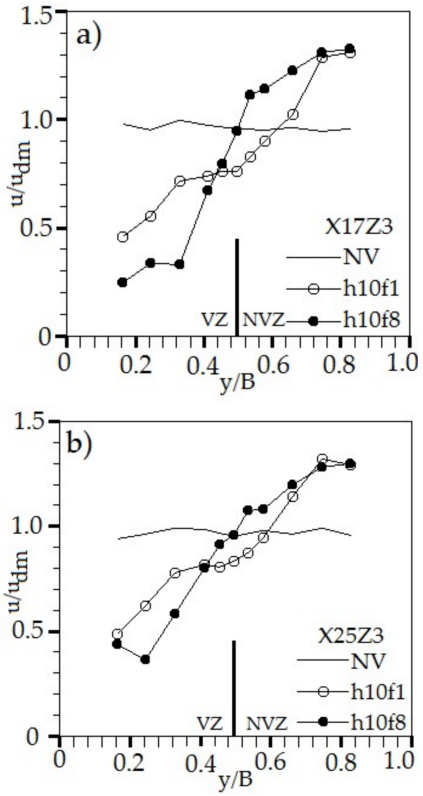

Figure 11. Non-dimensional streamwise velocity distributions along the spanwise direction at z/h_v = 0.5 for h_v = 0.1 m and different SVFs; (**a**) X17; (**b**) X25.

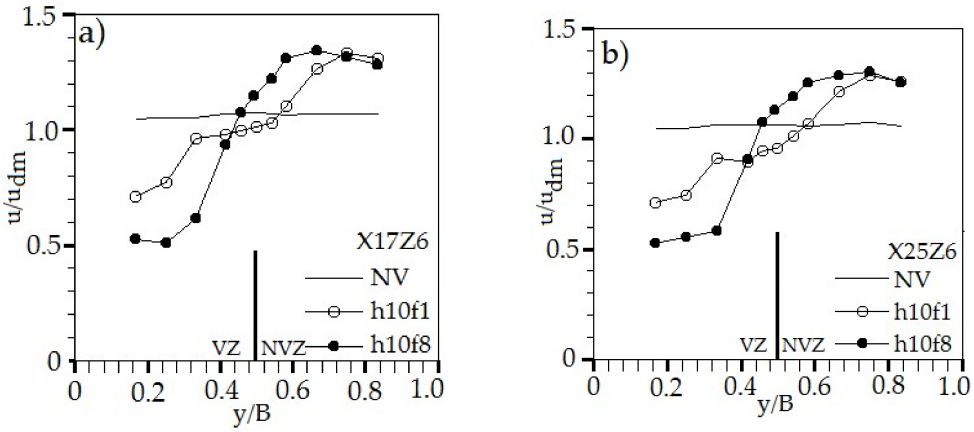

Figure 12. Non-dimensional streamwise velocity distributions along the spanwise direction at z/h_v = 1.25 for h_v = 0.1 m and different SVFs; (**a**) X17; (**b**) X25.

Meftah et al. [32] studied on flow patterns in partly obstructed channel. They used a rigid emergent vegetation layer to illustrate the obstruction in the channel. Density of the vegetated area was given as n = 400 cylinders/m^2 in their studies. They performed mid-depth velocity measurements using ADV in the experiments. They stated that the flow properties depend on contraction ratio (C_r) which is the ratio of the width of the obstructed area to the width of the unobstructed area. The results they obtained in the unobstructed area near the obstructed area and our results in the wake region of vegetation layer (data in Figure 11 where data correspond to the mid-depth of the vegetation layer) were plotted in Figure 13. Here, R1, R2, R3 and R4 correspond to C_r = 3.21, C_r = 1.05, C_r = 0.36 and C_r = 0.16, respectively. The contraction ratio was C_r = 0.94 in our study. In Figure 13, y′ starts at the

edge of the vegetation layer and B_{nv} is the width of the non-vegetated part. Velocity values near the edge are higher than Meftah et al. [32]'s velocity values. This is because our data were obtained in the wake region of the vegetation layer. Another important point was that an increasing velocity trendline occurred between $y'/B_{nv} = 0$ and $y'/B_{nv} = 0.5$ and the horizontal velocity trendline started at $y'/B_{nv} = 0.5$ for both of the studies. The horizontal velocity trendline of this study corresponds to R3 which has $C_r = 0.36$ contraction ratio.

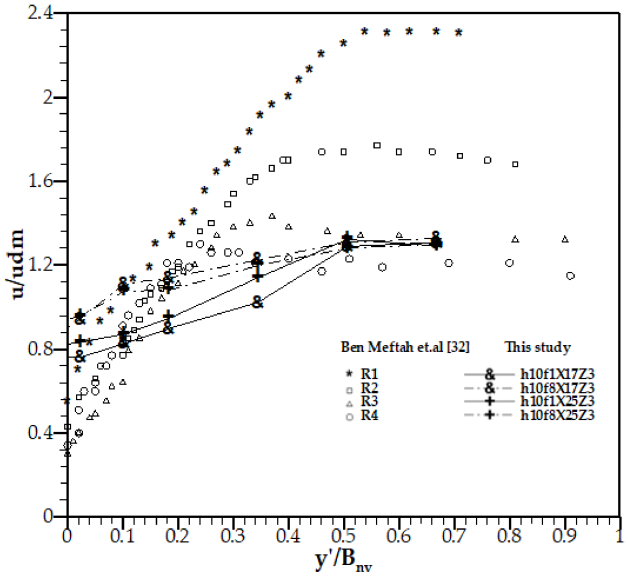

Figure 13. Transversal profiles of non-dimensional velocity distributions versus y/B_{nv}.

Figures 14 and 15 show the non-dimensional vertical velocity distributions at the top edge of the vegetation layer along the streamwise direction for $h_{v1} = 0.05$ m and $h_{v2} = 0.1$ m, respectively. Here, Y5, Y9, and Y13 corresponded to inside the vegetation layer, edge of the vegetation layer, and non-vegetated half part of the channel in spanwise direction, respectively. Vertical velocity had positive values in the non-vegetated half of the channel for all cases and had higher values for higher SVF ($\phi = 0.08$) than lower SVF ($\phi = 0.01$). Apart from this, the vertical velocity distribution showed different behavior for different SVFs at the vegetation layer. It had negative values along the streamwise direction for lower SVF ($\phi = 0.01$). Additionally, vertical velocity was positive in the vegetated layer and negative in the wake region of the vegetated layer and different from zero for higher SVFs in the vegetation layer.

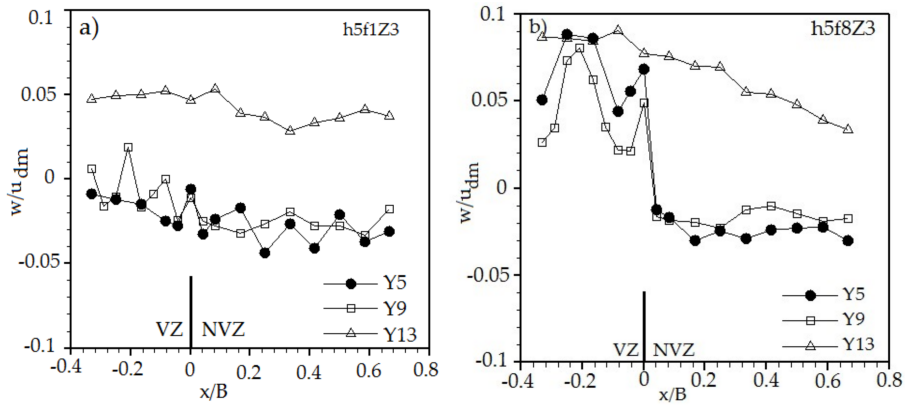

Figure 14. Non-dimensional vertical velocity distributions along the streamwise direction at $z/h_v = 1$ for $h_v = 0.05$ m; (**a**) $\phi = 0.01$; (**b**) $\phi = 0.08$.

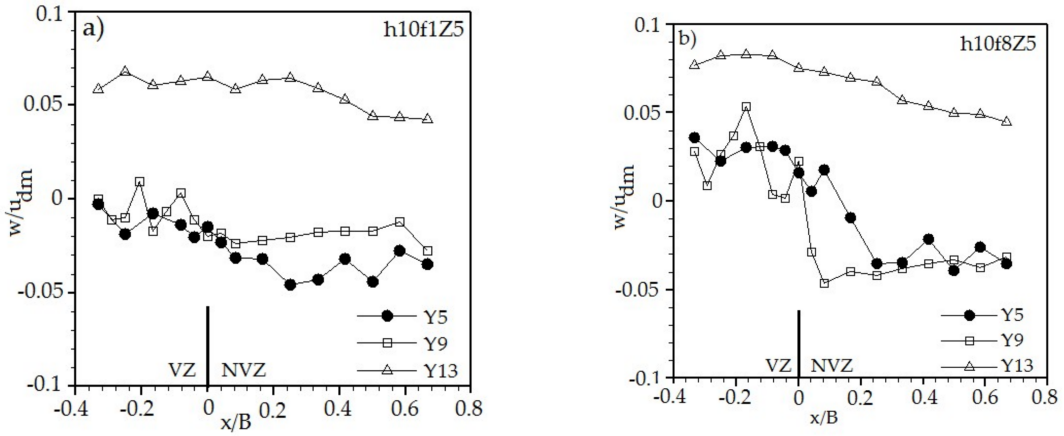

Figure 15. Non-dimensional vertical velocity distributions along the streamwise direction at $z/h_v = 1$ for $h_v = 0.1$ m; (**a**) $\phi = 0.01$; (**b**) $\phi = 0.08$.

In Figure 16, the non-dimensional Reynolds Stresses ($u'w'$) at the top edge of the vegetation layer along the Y5 section are shown for all cases. It was evident that higher vegetation SVF caused higher Reynolds Stress, which was significant for higher vegetation height. The Reynolds Stress ($u'w'$) showed a decreasing trend along the wake region for all cases. This result was consistent with the fact that canopies with $\lambda = ah \geq 0.1$ provided sufficient resistance to generate the vegetation shear layer downstream of the patch (see [33]).

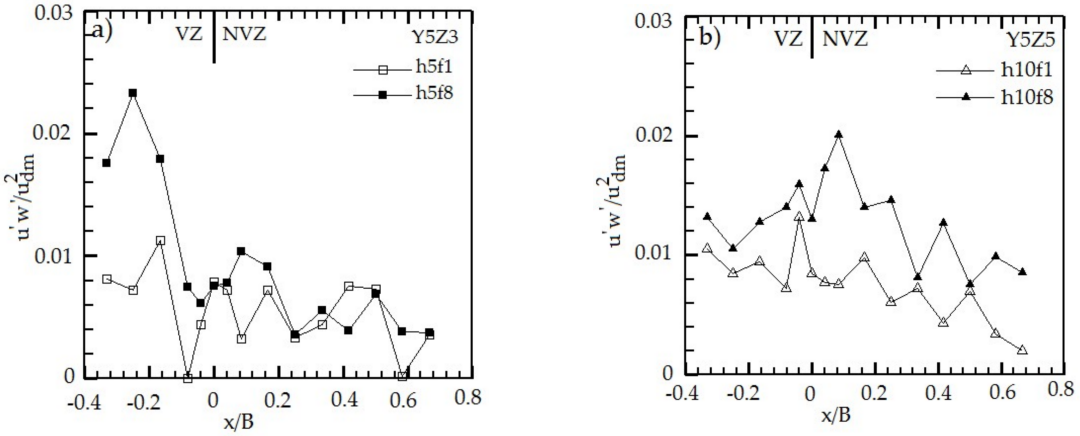

Figure 16. Non-dimensional Reynolds stresses along Y5 section for all cases; (**a**) h_v = 0.05 m; (**b**) h_v = 0.1 m.

White and Nepf (2007) [19] found that the peak of the turbulence intensity in the vegetation layer occurred in the vicinity of the junction between the vegetated and unvegetated parts of the channel at the partially obstructed channels. Here, the effects of vegetation height on the Reynolds stresses ($u'w'$) inside the vegetation and at the wake region were also investigated. For this purpose, the Reynolds stresses at the top edge of the vegetation at two different spanwise directions for denser cases were plotted (Figure 17). In Figure 17, X5 and X19 correspond to inside of the vegetation layer and the wake region of it, respectively. It was observed that in both sections, a higher vegetation layer caused higher shear stress at the top of the vegetation layer. The other important result was that vegetation affected the non-vegetated half of the channel until some point at X5 (Figure 17a). However, the vegetation did not affect the non-vegetated half of the channel in the wake region (Figure 17b).

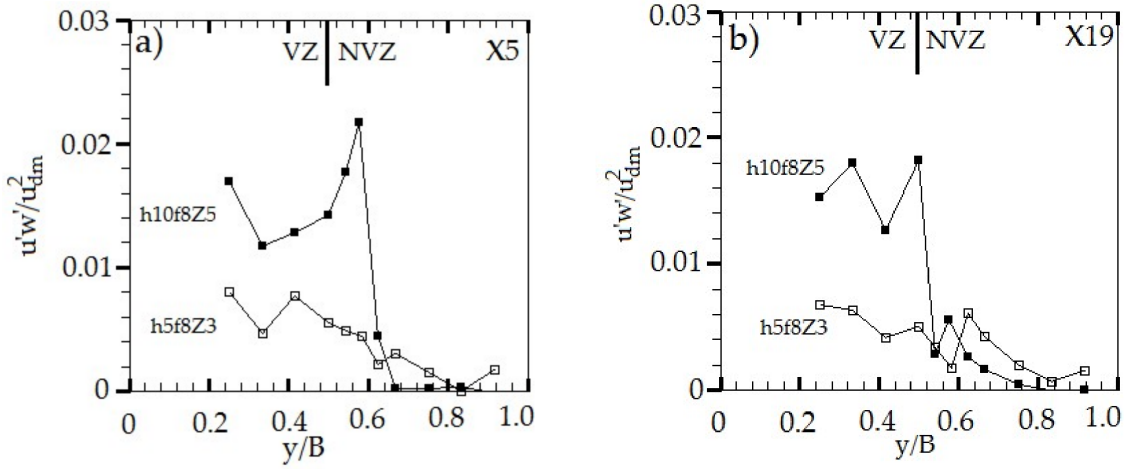

Figure 17. Non-dimensional Reynolds stresses distribution at the top edge of the vegetation layer along the spanwise direction; (**a**) X5; (**b**) X19.

4. Conclusions

In this study, the effect of a finite-length vegetation patch placed across half of the channel on the flow structure was examined. The study mainly focused on the wake region of the vegetative patch. For this purpose, an experimental study with different submergence ratios and SVFs was carried out.

It was observed that the vegetation layer decreased velocity both inside the vegetation layer and also in the wake region. Additionally, the velocity difference increased between the vegetated and non-vegetated cases, which was higher for higher vegetation height even when both cases had the same SVF. Different vegetation heights affected the velocity distribution in a different way, for example, low SVF had little effect on the velocity distribution over the vegetation layer while higher SVF had a large effect, which was an important decrease in the velocity distribution along the cross-section of the channel for h_{v1} = 0.05 m vegetation height. However, with the higher vegetation height (h_{v2} = 0.10 m), the vegetation layer affected the velocity distribution both within and over the vegetation layer. The velocity distribution over the cross-sections had inflectional velocity distribution for both vegetation heights. This type of velocity distribution implied that jet flow occurred in the non-vegetated half of the channel.

In addition, the vertical velocity distribution was also examined, and it was found that different behaviors for different SVFs were present at the vegetation layer. Moreover, vertical velocity was positive in the vegetated layer and negative in the wake region of vegetated layer.

Furthermore, the Reynolds Stress ($u'w'$) distribution was also investigated. It was demonstrated that higher SVF caused higher Reynolds stresses, which was significant for higher vegetation height at the edge of the vegetation layer. The Reynolds Stresses ($u'w'$) also displayed a decreasing trend along the wake region for all cases.

Acknowledgments: The authors would like to acknowledge the funding of the research project (MF-17008) from Adnan Menderes University (ADU). The authors would also like to thank the ADU Civil Engineering Department students Canberk Karacasu and Rıdvan Sarıgül who helped during the experiments.

Author Contributions: Didem Yılmazer, Ayşe Yüksel Ozan and Kubilay Cihan conceived and designed the experiments; Didem Yılmazer, Ayşe Yüksel Ozan and Kubilay Cihan performed the experiments; Didem Yılmazer, Ayşe Yüksel Ozan and Kubilay Cihan analyzed the data; Ayşe Yüksel Ozan wrote the paper. All authors read and approved the final manuscript.

Conflicts of Interest: The authors declare no conflict of interest.

References

1. Fonseca, M.S.; Kenworthy, W.J. Effects of current on photosynthesis and distribution of seagrasses. *Aquat. Bot.* **1987**, *27*, 59–78. [CrossRef]
2. Nepf, H.M. Drag, turbulence, and diffusion in flow through emergent vegetation. *Water Resour.* **1999**, *35*, 479–489. [CrossRef]
3. Gambi, M.C.; Nowell, A.R.M.; Jumars, P.A. Flume observations on flow dynamics in *Zostera marina* (eelgrass) beds. *Mar. Ecol. Prog. Ser.* **1990**, *61*, 159–169. [CrossRef]
4. Vivoni, E.R. Turbulence Structure of a Model Seagrass Meadow. Ph.D. Thesis, Massachusetts Institute of Technology, Cambridge, UK, 1998.
5. Wallace, S.; Luketina, D.; Cox, R. Large scale turbulence in seagrass canopies. In Proceedings of the 13th Australasian Fluid Mechanics Conference, Melbourne, Australia, 13–18 December 1998.
6. Raupach, M.R.; Shaw, R.H. Averaging procedures for flow within vegetation canopies. *Bound. Layer Meteorol.* **1982**, *22*, 79–90. [CrossRef]
7. Gao, W.; Shaw, R.H.; Paw, U.K.T. Observation of organized structure in turbulent flow within and above a forest canopy. *Bound. Layer Meteorol.* **1989**, *47*, 349–377. [CrossRef]
8. Raupach, M.R.; Finnigan, J.J.; Brunet, Y. Coherent eddies and turbulence in vegetation canopies: The mixing layer analogy. *Bound. Layer Meteorol.* **1996**, *78*, 351–382. [CrossRef]
9. Ikeda, S.; Kanazawa, M. Three-dimensional organized vortices above flexible water plants. *J. Hydraul. Eng.* **1996**, *122*, 634–640. [CrossRef]
10. Okamoto, T.; Nezu, I. Spatial evolution of coherent motions in finite-length vegetation patch flow. *Environ. Fluid Mech.* **2013**, *13*, 417–434. [CrossRef]
11. Ghisalberti, M.; Nepf, H.M. The structure of the shear layer in flows over rigid and flexible canopies. *Environ. Fluid Mech.* **2006**, *6*, 277–301. [CrossRef]
12. Ghisalberti, M.; Nepf, H.M. The limited growth of vegetated shear layers. *Water Resour. Res.* **2004**, *40*, W07502. [CrossRef]
13. Ben Meftah, M.; De Serio, F.; Mossa, M. Hydrodynamic behaviour in the outer shear layer of partly obstructed open channels. *Phys. Fluids* **2014**, *26*, 065102. [CrossRef]
14. Ben Meftah, M.; Mossa, M. Partially obstructed channel: Contraction effect on the flow hydrodynamic structure and prediction of the transversal mean velocity profile. *J. Hydrol.* **2016**, *542*, 87–100. [CrossRef]
15. Nepf, H.M.; Vivoni, E.R. Flow structure in depth-limited, vegetated flow. *J. Geophys. Res.* **2000**, *105*, 28547–28557. [CrossRef]
16. Poggi, D.; Porporato, A.; Ridolfi, L.; Albertson, J.D.; Katul, G.G. The Effect of Vegetation Density on Canopy Sun-Layer Turbulence. *Bound. Layer Meteorol.* **2004**, *111*, 565–587. [CrossRef]
17. Brito, M.; Fernandes, J.; Leal, J.B. Porous media approach for RANS simulation of compound open-channel flows with submerged vegetated floodplains. *Environ. Fluid Mech.* **2016**, *16*, 1247–1266. [CrossRef]
18. Kang, H.; Choi, S.U. Turbulence modeling of compound open-channel flows with and without vegetation on the floodplain using the Reynolds stress model. *Adv. Water Resour.* **2006**, *29*, 1650–1664. [CrossRef]
19. White, B.L.; Nepf, H.M. Shear instability and coherent structures in shallow flow adjacent to a porous layer. *J. Fluid Mech.* **2007**, *593*, 1–32. [CrossRef]
20. Kaimal, J.; Finnigan, J. *Atmospheric Boundary Layer Flows*; Oxford University Press: New York, NY, USA, 1994.
21. Schlichting, H. *Boundary Layer Theory*, 7th ed.; McGraw-Hill: New York, NY, USA, 1979.
22. Kamphuis, J.W. Determination of sand roughness for fixed beds. *J. Hydraul. Res.* **1974**, *12*, 193–203. [CrossRef]
23. Fredsoe, J.; Andersen, K.H.; Sumer, B.M. Wave plus current over a ripple-covered bed. *Coast. Eng.* **1999**, *38*, 177–221. [CrossRef]
24. SonTek. ADV Field Technical Manual. In *SonTek Technical Documentation*; SonTek/YSI Inc.: San Diego, CA, USA, 2001.
25. Goring, D.G.; Nikora, V.I. Despiking Acoustic Doppler Velocimeter Data. *J. Hydraul. Eng.* **2002**, *128*, 117–126. [CrossRef]
26. Wahl, T.L. Analyzing ADV data using WinADV. In Proceedings of the Joint Conference on Water Resource Engineering and Water Resources Planning and Management, Minneapolis, MN, USA, 30 July–2 August 2000.

27. Ben Meftah, M.; Mossa, M.A. A modified log-law of flow velocity distribution in partly obstructed open channels. *Environ. Fluid Mech.* **2016**, *16*, 453–479. [CrossRef]
28. Nezu, I.; Onitsuka, K. Turbulent structures in partly vegetated open-channel flows with LDA and PIV measurements. *J. Hydraul. Res.* **2001**, *39*, 629–642. [CrossRef]
29. Yang, K.; Cao, S.; Knight, D.; Flow, P. Flow patterns in compound channels with vegetated floodplains. *J. Hydraul. Eng.* **2007**, *133*, 148–159. [CrossRef]
30. Ikeda, S.; Ohta, K.; Hasegawa, H. Periodic vortices at the boundary of vegetated area along river bank. *J. Hydraul. Coast. Environ. Eng. JSCE* **1992**, *443*, 47–54. (In Japanese) [CrossRef]
31. Ikeda, S.; Kanazawa, N.; Ohta, K. Flow over flexible vegetation and 3-D structure of organized vortex associated with honami. *J. Hydraul. Coast. Environ. Eng. JSCE* **1995**, *515*, 33–43. (In Japanese) [CrossRef]
32. Ben Meftah, M.; De Serio, F.; Malcangio, D.; Mossa, M. Resistance and boundary shear in a partly obstructed channel flow. In *River Flow*; Taylor & Francis Group: London, UK, 2016; pp. 795–801.
33. Nepf, H. Hydrodynamics of vegetated channels. *J. Hydraul. Res.* **2012**, *50*, 262–279. [CrossRef]